Science of the Total Environment 829 (2022) 154607

Contents lists available at ScienceDirect

Science of the Total Environment

journal homepage: www.elsevier.com/locate/scitotenv

The striking effect of vertical mixing in the planetary boundary layer on new particle formation in the Yangtze River Delta

Shiyi Lai [a,b,1], Shangfei Hai [a,1], Yang Gao [c,d,*], Yuhang Wang [e,**], Lifang Sheng [a], Aura Lupascu [f], Aijun Ding [b], Wei Nie [b], Ximeng Qi [b], Xin Huang [b], Xuguang Chi [b], Chun Zhao [g,h], Bin Zhao [i,j], Manish Shrivastava [k], Jerome D. Fast [k], Xiaohong Yao [c,d], Huiwang Gao [c,d]

[a] College of Oceanic and Atmospheric Sciences, Ocean University of China, Qingdao 266100, China
[b] School of Atmospheric Sciences, Nanjing University, Nanjing 210023, China
[c] Frontiers Science Center for Deep Ocean Multispheres and Earth System, and Key Laboratory of Marine Environment and Ecology, Ministry of Education, Ocean University of China, Qingdao 266100, China
[d] Qingdao National Laboratory for Marine Science and Technology, Qingdao 266100, China
[e] School of Earth and Atmospheric Sciences, Georgia Institute of Technology, Atlanta, GA 30332, USA
[f] Institute for Advanced Sustainability Studies, Potsdam D-14467, Germany
[g] School of Earth and Space Sciences, University of Science and Technology of China, Hefei, China
[h] CAS Center for Excellence in Comparative Planetology, University of Science and Technology of China, Hefei, China
[i] State Key Joint Laboratory of Environment Simulation and Pollution Control, School of Environment, Tsinghua University, Beijing 100084, China
[j] State Environmental Protection Key Laboratory of Sources and Control of Air Pollution Complex, Beijing 100084, China
[k] Atmospheric Sciences and Global Change Division, Pacific Northwest National Laboratory, Richland, WA 99354, USA

HIGHLIGHTS

- NPF in the top of the boundary layer may start earlier than that in the surface.
- The aerosol vertical mixing plays a large role in the surface particle number.
- The vertical transport from NPF aloft may trigger the particle growth in the surface.

GRAPHICAL ABSTRACT

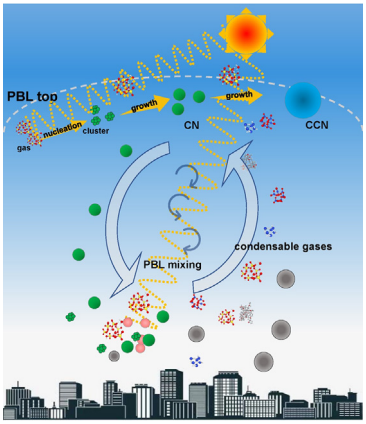

ARTICLE INFO

Article history:
Received 20 December 2021
Received in revised form 13 February 2022
Accepted 12 March 2022
Available online 17 March 2022

ABSTRACT

New particle formation (NPF) induces a sharp increase in ultrafine particle number concentrations and potentially acts as an important source of cloud condensation nuclei (CCN). As the densely populated area of China, the Yangtze River Delta (YRD) region shows a high frequency of observed NPF events at the ground level, especially in spring. Although recent observational studies suggested a possible connection between NPF at the higher altitudes and ground level, the

* Correspondence to: Y. Gao, Frontiers Science Center for Deep Ocean Multispheres and Earth System, and Key Laboratory of Marine Environment and Ecology, Ministry of Education, Ocean University of China, Qingdao 266100, China.
** Corresponding author.
E-mail addresses: yanggao@ouc.edu.cn (Y. Gao), yuhang.wang@eas.gatech.edu (Y. Wang).
[1] Authors contributed equally to this study.

http://dx.doi.org/10.1016/j.scitotenv.2022.154607

Editor: Pingqing Fu

Keywords:
New particle formation
Cloud condensation nuclei
NPF-explicit WRF-Chem
Vertical mixing of aerosols

role played by vertical mixing, particularly in the planetary boundary layer (PBL) is not fully understood. Here we integrate measurements in Nanjing on 15–20 April 2018, and the NPF-explicit Weather Research and Forecast coupled with chemistry (WRF-Chem) model simulations to better understand the governing mechanisms of the NPF and CCN. Our results indicate that newly formed particles at the boundary layer top could be transported downward by vertical mixing as the PBL develops. A numerical sensitivity simulation created by eliminating aerosol vertical mixing suppresses both the downward transport of particles formed at a higher altitude and the dilution of particles at the ground level. The resulting higher Fuchs surface area at the ground level, together with the lack of downward transport, yields a sharp weakening of NPF strength and delayed start of NPF therein. The aerosol vertical mixing, therefore, leads to a more than double increase of surface $CN_{10–40}$ and a one third decrease of boundary layer top $CN_{10–40}$. Additionally, the continuous growth of nucleated ultrafine particles at the boundary layer top is strongly steered by the upward transport of condensable gases, with close to half increase of particle number concentrations in Aitken mode and CCN at a supersaturation rate of 0.75%. The findings may bridge the gap in understanding the complex interaction between PBL dynamics and NPF events, reducing the uncertainty in assessing the climate impact of aerosols.

1. Introduction

New particle formation (NPF) is an important secondary source of particles in the atmosphere, characterized by a dramatic sharp increase in ultrafine particle concentrations (less than 100 nm). Particles with a diameter greater than 50 nm, which can act as cloud condensation nuclei (CCN), affect the climate by changing cloud properties and precipitation (Dusek et al., 2006; Solomon et al., 2007). Several studies have shown that aerosol indirect forcing is sensitive to NPF (Wang and Penner, 2009; Yu and Luo, 2009; Kazil et al., 2010). For example, Wang and Penner (2009) noted that the inclusion of the nucleation process in the global model greatly affects the estimation of the radiative forcing with a range of -1.22 to $-2.03\ \mathrm{Wm}^{-2}$. Precursor gas molecules form critical molecular clusters with a diameter of ~1 nm through nucleation. Some of the newly formed particles further grow through condensation and coagulation (Kulmala, 2003; Zhang et al., 2012).

The determination of nucleating species is one of the key points of the nucleation mechanism. The majority of early studies focused on the nucleation of gaseous sulfuric acid since the saturation vapor pressure of gaseous sulfuric acid is rather low, and sulfate is a major component of nucleation mode particles. However, gaseous sulfuric acid alone cannot explain the observed particle formation rates in some cases (Turco et al., 1998; O'Dowd et al., 2002; Kulmala et al., 2016). Other precursors have been proposed as being involved in the formation of the critical nucleus under different environments, such as ammonia (Kirkby et al., 2011), amines (Yao et al., 2018), oxidized organic vapors (Schobesberger et al., 2013; Riccobono et al., 2014), and iodine oxides especially in marine and coastal planetary boundary layer (PBL) (O'Dowd et al., 2002).

Observations have shown that NPF events take place not only at the surface but also in the free troposphere, which has favorable conditions for the onset of NPF such as sufficient sun exposure and cosmic rays, enough condensable vapors, low temperature, and low pre-existing aerosol surface area (Lee et al., 2003; Boulon et al., 2011; Rose et al., 2015; Qi et al., 2019; Zhao et al., 2020). NPF events have also been observed in the turbulent zones of the residual layer (nighttime) and near the entrainment zone (daytime) (Stratmann et al., 2003; Wehner et al., 2010; Platis et al., 2016). Based on limited observations, a possible connection between NPF and PBL dynamics has been proposed. Several field observations confirmed that NPF may proceed during the PBL development rather than a ground-level phenomenon (Stratmann et al., 2003; Wehner et al., 2010; Bianchi et al., 2016). It is very likely that newly formed particles observed at the surface have been nucleated at higher altitudes and mixed downwards (Crumeyrolle et al., 2010; Wehner et al., 2010; Platis et al., 2016). As an extreme case, the secondary particles generated at the high free troposphere (6–8 km) would significantly increase CCN at a lower altitude when descending towards the surface in the clean marine atmosphere with the low condensation sink (Williamson et al., 2019). However, modeling NPF in polluted atmospheres is still limited, particularly for the relationship between PBL dynamics and NPF and CCN. In this study, with the budget diagnostics for dry deposition (including dry deposition, vertical mixing, activation of particles) tendencies available in the model, we are able to better illustrate and understand how each process influences the NPF events and CCN.

Many studies have been conducted to evaluate the application of various nucleation parameterizations through numerical experiments in global and regional models (Matsui et al., 2011; Westervelt et al., 2014; Lupascu et al., 2015; Dunne et al., 2016; Chen et al., 2019; Fanourgakis et al., 2019; Zhao et al., 2020). Westervelt et al. (2014) used the Goddard Earth Observing System global chemical transport model (GEOS-Chem) coupled to the two-moment aerosol sectional (TOMAS) scheme with eight nucleation mechanisms (or prefactors) and found that the $CCN_{0.2\%}$ over the boundary layer can be enhanced by 49% to 78% due to nucleation. Matsui et al. (2011) introduced activation (ACT) and kinetic (KIN) parameterizations into the Weather Research and Forecast coupled with chemistry (WRF-Chem) model and found that NPF contributed 20%–30% to the CN_{10} (>10 nm in diameter) concentrations in Beijing and its surrounding areas. The study of Lupascu et al. (2015) showed that the ACT parameterization performed the best among different nucleation parameterizations in comparison with observational data from the Carbonaceous Aerosol and Radiative Effects Study (CARES) carried out in northern California during June 2010.

As one of the most densely populated and urbanized parts of China, the Yangtze River Delta (YRD) shows high frequency and formation rates of NPF events (Herrmann et al., 2014; Qi et al., 2015; Chu et al., 2019). Based on the long term measurements (December 2011 to November 2013) at the Station for Observing Regional Processes of the Earth System (SORPES) in Nanjing, which is a megacity in the YRD city cluster, Qi et al. (2015) noted that NPF occurs most frequently in spring with a frequency of 44%. This finding was consistent with other studies conducted in the YRD (Zhu et al., 2013; Leng et al., 2014). Furthermore, NPF events around the top of the PBL in the YRD have recently been reported by Qi et al. (2019), as was the case in other studies (Stratmann et al., 2003; Wehner et al., 2010; Platis et al., 2016; Chen et al., 2018; Lampilahti et al., 2020). As suggested by several earlier studies, the NPF observed in the residual or inversion layer could be connected to the NPF at ground level (Stratmann et al., 2003; Wehner et al., 2010; Platis et al., 2016; Chen et al., 2018; Lampilahti et al., 2020).

In this study, based on the NPF-explicit WRF-Chem model and comprehensive analysis with field observational data at SORPES, we investigated the characteristics of NPF events in Nanjing in the spring of 2018. The effects of vertical mixing on the redistribution and growth of the secondary particles to the CCN size at the surface and the boundary layer top were fully investigated with the aid of a model.

2. Data and methods

2.1. Observations

In this study, the field observation site is located at SORPES (118°57′10″ E, 32°07′14″N) in the Xianlin Campus of Nanjing University. SORPES is a suburban station with an altitude of 40 m and is considered a regional background station in the Yangtze River Delta (YRD) region (Ding et al., 2013).

SORPES is equipped with ThermoTEI 43i for SO_2 observation. $PM_{2.5}$ was measured with a combined technique of light scattering photometry and beta radiation attenuation (Thermo Scientific SHARP Monitor Model 5030) at SORPES. A CCN counter was employed to monitor CCN concentrations at several different supersaturations (SS = 0.15%, 0.35%, 0.55% and 0.75%). Gaseous sulfuric acid, monoterpene and isoprene, which are closely associated with the modulation of new particle formation and growth, were observed by chemical ionization mass spectrometer (CIMS) and proton transfer reaction time-of-flight mass spectrometry (PTR-ToF-MS). In this study, two sets of instruments were used to measure the aerosol particle size distribution, a Differential Mobility Particle Sizer (DMPS) for the size range of 6–800 nm and a Particle Size Magnifier (PSM) for the 1.2–2.5 nm size distribution (Qi et al., 2015). Note that there is a measurement gap in the size range of 2.5 nm to 6 nm in this study, which could be fulfilled in the future by instruments such as Neutral cluster and Air Ion Spectrometers (NAIS) (Kulmala et al., 2007; Manninen et al., 2009). All the data were continuously measured at SORPES. The meteorological parameters, e.g., air temperature, relative humidity, wind direction, and wind speed, were obtained from the University of Wyoming website (http://www.weather.uwyo.edu/surface/). The ambient air monitoring data, including $PM_{2.5}$ and SO_2, were acquired from the China National Environmental Monitoring Centre.

2.2. Model configurations and settings

In this study, version 3.9 of the WRF-Chem model (Grell et al., 2005; Fast et al., 2006) was used to simulate NPF events and their effects on the aerosol particle size distribution as well as CCN. The simulation was conducted on 7–20 April 2018, with the first seven days as the model spin-up time. The model domain covered most of mainland China and its surrounding area, centered at 34°N, 110°E with a 36 km horizontal resolution. The projection method was Lambert Conformal Conic Projection, and the two standard latitudes were 25°N and 40°N. There were 35 vertical layers from the ground level to 50 hPa. The key parameterization options used in this study include the unified Noah land surface scheme (Chen and Dudhia, 2001; Tewari et al., 2004), the Monin-Obukhov surface layer scheme (Jimenez et al., 2012), the Morrison microphysics scheme (Morrison et al., 2009), the Grell-3D cumulus parameterization scheme (Grell, 1993), the Yonsei University (YSU) boundary layer scheme (Hong et al., 2006), and the Rapid Radiative Transfer Model for General Circulation Models (RRTMG) longwave and shortwave radiation (Iacono et al., 2008). The Statewide Air Pollution Research Center (SAPRC-99) mechanism (Carter, 2000) and Model for Simulating Aerosol Interactions and Chemistry (MOSAIC) module (Zaveri et al., 2008) were used to represent gas phase and aerosol chemistry, respectively.

The National Centers for Environmental Prediction (NCEP) Climate Forecast System Version 2 (CFSv2) (Saha et al., 2014) 6-hourly products with a 0.5° × 0.5° spatial resolution were used as the initial and boundary conditions of meteorological fields. Anthropogenic emissions were derived from the Multi-resolution Emission Inventory for China 2016 at 0.25° × 0.25° horizontal resolution (MEIC-2016 database, see www.meicmodel.org). The 2.04 version of the Model of Emissions of Gases and Aerosols from Nature (MEGAN v2.04) with the Moderate Resolution Imagine Spectroradiometer (MODIS) land cover for 2016 embedded in WRF-Chem was used to calculate biogenic emissions online (Guenther et al., 2006). Please note that biogenic emissions from urban green spaces as well as their modulation of NPF events through interactions with anthropogenic emissions are not considered in this study, which may deserve to be elucidated in future studies (Ma et al., 2019; Gao et al., 2021; Ma et al., 2022). The initial and boundary conditions of WRF-Chem were provided by the results from the Community Atmosphere Model with Chemistry (CAM-Chem).

In the commonly used version of WRF-Chem, the Model for Simulating Aerosol Interactions and Chemistry (MOSAIC) aerosol module divides aerosols ranging from 39 nm to 10 μm into 4 or 8 sectional bins. This size range cannot capture freshly nucleated particles with a diameter of a few nanometers. In this study, the updated MOSAIC module with a new sectional framework option was adopted, using 20 bins spanning 1 nm to 10 μm (Matsui et al., 2011; Matsui et al., 2013; Cui et al., 2014; Lupascu et al., 2015). The simplified 2-species volatility basis-set (VBS) mechanism for primary organic aerosol (POA) and nontraditional secondary organic aerosol (SOA), with an additional 1-species treatment of traditional SOA, was used to model the evolution of organic aerosol (Shrivastava et al., 2011). The POA was treated based on two volatility species with saturation vapor concentrations (C*) of 10^{-2} and 10^{5} μg m^{-3} (at 298 K and 1 atm). The C* of traditional and nontraditional SOAs was set as 1 μg m^{-3} and 10^{-2} μg m^{-3}, respectively, while the nontraditional SOAs were primarily formed due to the oxidation of semivolatile and intermediate volatility organic compounds. The current nucleation mechanism mostly involves H_2SO_4 and highly oxygenated multifunctional compounds (HOMs) (Schobesberger et al., 2013; Riccobono et al., 2014). The linear regression between sub-3 nm particle number concentrations and different precursors, including H_2SO_4 and the oxidation products of monoterpene and isoprene, which are important precursors for HOMs (Sipila et al., 2010; Surratt et al., 2010; Lin et al., 2013; Ehn et al., 2014; Brean et al., 2019), reveals that H_2SO_4 alone shows the highest correlation with sub-3 nm particle number concentrations (Section S1 and Fig. S1 in the Supplementary Information). Thus, in this study, the ACT mechanism was implemented, with the equation shown below.

$$\mathrm{ACT}: J^* = K_{ACT} \bullet [H_2SO_4] \tag{1}$$

J^* is the formation rate of particles at 1 nm (cm^{-3} s^{-1}), and [H_2SO_4] represents the concentration of gaseous sulfuric acid (cm^{-3}). Coefficients K_{ACT} derived from observations in different locations could span 3–4 orders of magnitude. In this study, $K_{ACT} = 2 \times 10^{-7}$ s^{-1} was used as the base case, the same as the previous studies in Matsui et al. (2011) and Matsui et al. (2013).

To investigate how the vertical mixing of gas and aerosol affects NPF and CCN, two experiments were conducted by turning off the vertical mixing of gases (Ex_GM) and aerosol (Ex_AM). WRF tended to underestimate PBL mixing at night, which then led to high $PM_{2.5}$ concentrations at the ground level due to limited vertical mixing (Du et al., 2020). Therefore, the minimum PBL mixing coefficient was increased from 0.1 to 5 m^2 s^{-1} following Du et al. (2020). After the modification, the diurnal variation in $PM_{2.5}$ was much more accurately reproduced (Section S2 and Fig. S2).

3. Results

3.1. Model evaluation

Meteorological conditions play substantial roles in modulating the NPF events. For instance, the wind speed is closely related to the atmospheric mixing capacity, thereby affecting the concentration of background aerosols and condensation sinks in the atmosphere (Kulmala et al., 2012). In this study, the hourly wind speed at 10 m (WS10), air temperature at 2 m (T2) and specific humidity at 2 m on 15–20 April 2018 were evaluated based on the data available at the University of Wyoming (http://www.weather.uwyo.edu/surface/). The statistical metrics, including mean bias (MB), mean gross error (ME), and root mean square deviation (RMSE), of

Table 1
Statistical analysis of the modeled 2-m temperature, specific humidity and 10-m wind speed for the base case (ACT experiment).

	Index		Benchmarks[a]
WS10 (m s^{-1})	RMSE	1.41	<2
	MB	0.67	<±0.5
T2 (K)	ME	2.14	<2
	MB	−1.79	<±0.5
Specific humidity (g kg^{-1})	ME	1.01	<2
	MB	−0.69	<±1

[a] Benchmarks are from Emery and Tai (2001) and Tesche et al. (2002).

the model evaluation are shown in Table 1, exhibiting reasonable performance compared with the benchmark value (Emery and Tai, 2001; Tesche et al., 2002), albeit with slight underestimation of near-surface air temperature.

The air quality dataset at the nine monitoring stations in Nanjing (Fig. S3), available from the China National Environmental Monitoring Centre (http://www.pm25.in, last access: 30 September 2020), was used to evaluate the WRF-Chem model in simulating the NPF relevant pollutants, mainly SO_2 and $PM_{2.5}$. While SO_2 is an important precursor of NPF, the $PM_{2.5}$ concentration may reflect to a certain extent the pre-existing particles in the atmosphere potentially acting as a condensation sink (CS), which is closely associated with the evolution of newly formed particles. Based on the mean fractional bias (MFB; 50%) and mean fractional error (MFE; 75%) suggested by the US EPA (2007), the simulated $PM_{2.5}$ concentration met the benchmarks, with MFB = 11% and MFE = 29%. In terms of SO_2, no benchmarks are available, and a general overprediction exists with MFB and MFE of 71% and 74%, respectively.

In addition, the observed H_2SO_4 from the SORPES site described earlier was used for comparison with the model results, implying an overall overestimation of 1 order of magnitude in WRF-Chem (Section S3 and Fig. S4). Overestimations in H_2SO_4 have been widely reported (Matsui et al., 2011; Cai et al., 2016; Yu et al., 2020). The key precursor SO_2 was overpredicted with MFB = 83% compared with the observation at the SORPES. Sensitivity numerical simulations through the reduction of SO_2 emissions by 90% and 70% were conducted. As shown in Fig. S4, the concentration of SO_2 was significantly underpredicted with an emission reduction of 90%, however, the concentration of H_2SO_4 was still overestimated. This result indicated that the overestimation of H_2SO_4 (Fig. S4) cannot be fully explained by SO_2, which may be attributed to either measurement bias as pointed out by Neitola et al. (2015) and Yu et al. (2020), or the missing heterogeneous reactions in MOSAIC associated with sulfate (Huang et al., 2014; Xie et al., 2015; Shang et al., 2020).

$CN_{10–40}$ (10–40 nm) were evaluated against measurements by DMPS at SORPES. They were reproduced with a correlation coefficient of 0.68 and by a factor of ~2, which was comparable to that of Matsui et al. (2013). In their model calculations, the same K_{ACT} coefficient of $2 \times 10^{-7}\ s^{-1}$ in the ACT parameterization was adopted to reproduce the NPF events in Beijing.

3.2. Observations and data analysis

As pointed out in Qi et al. (2015), the spring has the highest frequency in NPF events at the SORPES station based on the measurements from December 2011 to November 2013. April 15–20, 2018, was chosen as the study period. As depicted in Fig. 1a, on 15–20 April, six NPF events were captured by DMPS on a daily basis.

The PBL heights and mixing coefficients reflect the PBL mixing strength (Du et al., 2020). As shown in Fig. 1b, there was a clear diurnal variation with the maximum in the daytime. Strong PBL mixing and high PBLH occurred together in the first period (15–17 April), especially on 15 April and 16 April, with the maximum PBL mixing coefficients larger than 500 $m^2\ s^{-1}$. In contrast, in the latter period (18–20 April), the maximum PBL mixing coefficients were less than 400 $m^2\ s^{-1}$ with maximum coefficients of ~230 $m^2\ s^{-1}$ and ~100 $m^2\ s^{-1}$ on 19–20 April, respectively. As a consequence of weak PBL mixing, the Fuchs surface area (Section S4) during the latter period had an average value of 245 $\mu m^2\ cm^{-3}$ (the corresponding CS is ~0.033 s^{-1}) (Salma et al., 2016; Cai et al., 2017), which is comparable to other studies conducted in the YRD but an order higher than that measured at SMEAR II (Huang et al., 2016; Shen et al., 2016; Qi et al., 2018). During the latter period, the Fuchs surface areas were 30% higher than those in the first period (Section S5 and Fig. S5), implying a higher scavenging rate of precursor gases, clusters and newly formed particles (Kerminen et al., 2001; Deng et al., 2020). Although a low Fuchs surface area is more favorable for the onset of the NPF event (Herrmann et al., 2014), a banana-shaped particle number size distribution was still captured by DMPS during the latter period, and the growth of new particles was generally faster (Fig. 1a). As shown in Fig. 1c, sub-3 nm (red line in Fig. 1c) and nucleation mode (blue line in Fig. 1c) particle number concentrations in the first period show relatively high peaks compared with the latter period. However, the Aitken mode (yellow line in Fig. 1c) particle number concentrations

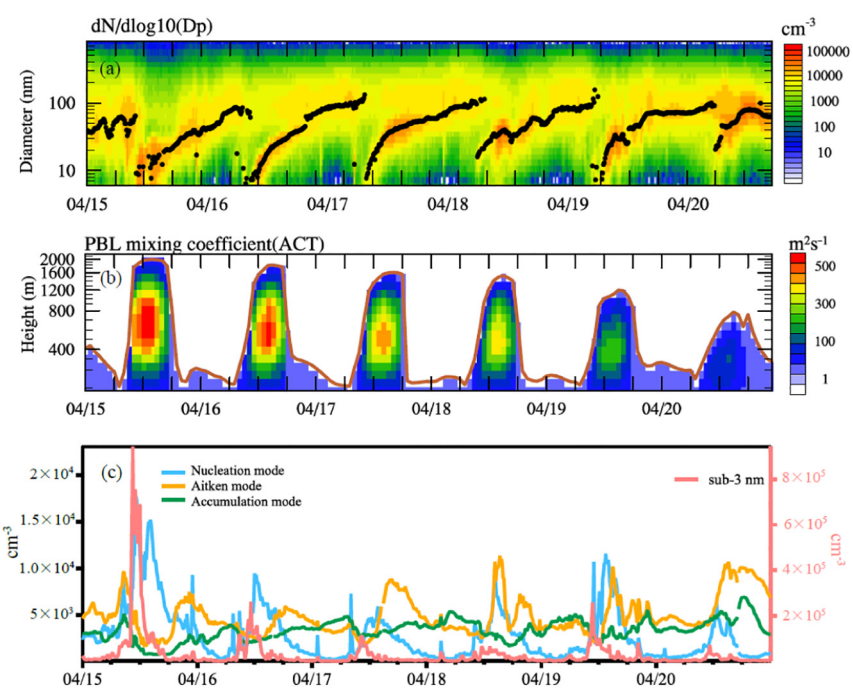

Fig. 1. Time series of observed particle number size distributions at SORPES from (a) 15–20 April. Black dots represent the representative diameters of the fitted mode (see details in the supplement). (b) Time series of the modeled mixing coefficient in the planetary boundary layer by the ACT experiment. The brown line denotes planetary boundary layer height (PBLH). (c) Times series of observed particle number concentrations in the nucleation mode (6–30 nm), Aitken mode (30–100 nm), accumulation mode (100–800 nm) and sub-3 nm particle number concentrations at the SORPES on 15–20 April. All time is the local standard time in this study.

showed comparatively higher peaks in the latter period relative to the first period, corresponding to 66% higher $GR_{6–30}$ (Section S4). In addition, on average, the sub-3 nm and nucleation mode particle number concentrations peaked at 10:40 (all time is the local standard time in this study) and 11:50 during the first period while the peak time showed up at 11:10 and 13:30 during the latter period, implicative of a delayed start time of NPF during the latter three days. Since there was stronger PBL mixing during the first period, it is speculated that there is an underlying relationship between the vertical mixing and NPF events at the ground. Since vertical observations are scarce and not available in this study, the model simulations were used to help reveal the impact of vertical mixing on NPF.

3.3. Influence of aerosol vertical mixing on CN

By comparing $CN_{10–40}$ in ACT and NUCOFF (the experiment without nucleation) experiments, it is found that nucleation contributed 88% to the surface $CN_{10–40}$ on average. Thus, $CN_{10–40}$ was used to discuss NPF events in this study. On 15–20 April, the modeled $CN_{10–40}$ at the boundary layer top and at ground level increased at almost the same time or slightly earlier (Fig. 2a). There was strong PBL mixing during the first three days (Fig. 1b), leading to a homogeneous distribution of newly formed particles in the PBL (Fig. 2a). However, on 18–20 April, accompanied by a decrease in vertical mixing, the PBLH also decreased (Fig. 1b). Weak PBL mixing led to a high Fuchs surface area at the surface (Fig. S6), thereby suppressing NPF and the growth of $CN_{10–40}$ therein by enhancing condensation and coagulation processes. Since the inversion layer at the boundary layer top tended to suppress the uplift of particles, PBL mixing encouraged the downward transport of newly formed particles transport downward with the development of the PBL (Fig. 2b). After the NPF started at the boundary layer top (Section S4), newly formed particles from the boundary layer top increased $CN_{10–40}$ at the ground level through PBL mixing (Fig. 2b). An analogous study by Xu et al. (2018) found that, based on vertical measurements and a modeling study, vertical mixing of aged plumes from the residual layer on surface O_3 concentration in Nanjing in the early morning was enhanced. The vertical dipole feature may last approximately 2 h, until the surface $CN_{10–40}$ began to grow (Fig. 2a). On these days, the modeled $CN_{10–40}$ at the boundary layer top started to increase earlier than at the ground level (Fig. 2a). It is noteworthy that the dipole structure of the vertical mixing appeared throughout the period on 15–20 April, with the signal more pronounced in the latter three days due primarily to the suppressed NPF at the surface resulting from weak PBL mixing.

To shed further light on how aerosol vertical mixing influences NPF at the ground level, an Ex_AM experiment was designed in which aerosol vertical mixing was turned off. During the first three days, $CN_{10–40}$ gradually became uniform in the vertical direction under the development of PBL as well as the enhanced PBL mixing (Figs. 2a, 3a–c). However, on the latter three days with comparatively weak PBL mixing, as demonstrated in Fig. 3d–f, there were peaks of $CN_{10–40}$ at the boundary layer top. In Ex_AM (dashed lines in Fig. 3), $CN_{10–40}$ at the boundary layer top increased substantially every day, with a distinctly higher $CN_{10–40}$ peak emerging at the boundary layer top compared with ACT. This could be additional evidence of ultrafine particles being transported downward. In Ex_AM, the maximum of $CN_{10–40}$ remained at the boundary layer top, where the $CN_{10–40}$ was much larger than that over the ground, with a magnitude of 10^5 cm^{-3}. On average, aerosol vertical mixing caused a 122% increase in $CN_{10–40}$ at the surface and a 64% reduction at the boundary layer top at 11:00–17:00. It is concluded that aerosol vertical mixing has an important impact on $CN_{10–40}$ near the ground.

Aerosol vertical mixing plays a crucial role in modulating the start time and the strength of NPF. For instance, NPF on 19 April started at 07:00 at the top of the boundary layer (Fig. 4a) while the start time was delayed 3 h at approximately 10:00 at the surface (Fig. 4c). By excluding the aerosol vertical mixing in the Ex_AM experiment, despite of little change in the start time of NPF at the top of the boundary layer (Fig. 4b vs. Fig. 4a), the enlarged Fuchs surface area (63% increase) as well as enhanced condensation and coagulation at the ground triggered a noticeable delay of 6 h at 16:00 in the appearance of nucleation-mode particles near the ground (Fig. 4d vs. Fig. 4c). Meanwhile, the elimination of aerosol vertical mixing yielded a sharp weakening of NMINP (Section S4) from the original value of 2.5×10^4 cm^{-3} to 0.8×10^4 cm^{-3}. The underlying mechanism of aerosol vertical mixing in triggering the earlier start of NPF is likely associated with the decrease in the condensation sink at the surface along with the development of PBL (Herrmann et al., 2014; Huang et al., 2016; Wu et al., 2020) and strengthened downward transport from the top of the boundary.

3.4. Influence of vertical mixing on CCN at the top of the PBL

Newly formed particles can potentially be activated as CCN after hours of growth (Zhu et al., 2014; Gao et al., 2020) and exert an important influence on the climate by altering the characteristics of cloud and precipitation processes. Thus, we concentrated on 12:00–18:00 in this section. The modeled CCN is slightly higher than the observations (MB = 178 cm^{-3}, 1262 cm^{-3}, 2280 cm^{-3}, 2279 cm^{-3} at supersaturations of 0.15%, 0.35%, 0.55% and 0.75%, respectively) (Fig. S6).

3.4.1. The impact of nucleation on the CCN at the top of the PBL

As discussed in Section 3.2, there was a relatively low PBLH on 18–20 April, which indicated weak vertical mixing. Thus, it is difficult for small particles formed at the boundary layer top to be transported downward, leading to the appearance of high $CN_{40–100}$ and CCN number concentration layer near the boundary layer top (Fig. 5a–b). The high CCN layer (denotes the layer in which the CCN number concentration exceeds 95% of the maximum value in the PBL; a similar definition for the high $CN_{40–100}$ layer) appears approximately 4–5 h after the occurrence of NPF nearby (Fig. 5b). It

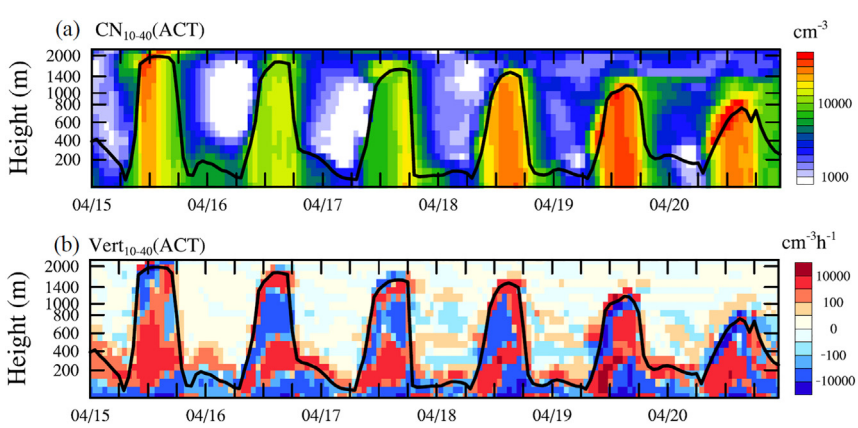

Fig. 2. Modeled time series by ACT experiment of (a) $CN_{10–40}$, (b) vertical mixing (includes dry deposition at the first layer) tendencies for particle number concentrations in the 10–40 nm diameter range. Note: black solid line denotes PBLH.

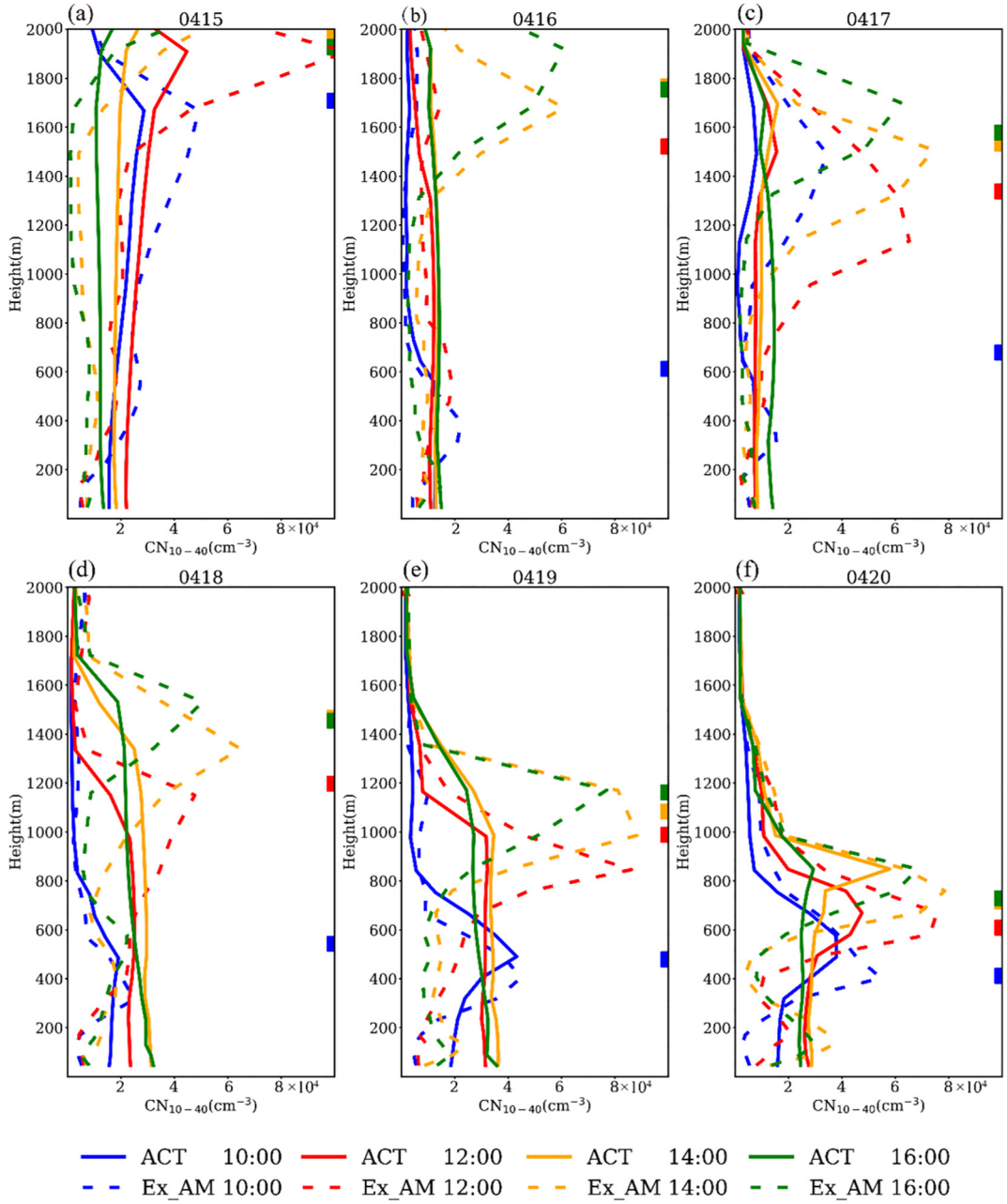

Fig. 3. Vertical profiles of $CN_{10–40}$ on (a) 15 April, (b) 16 April, (c) 17 April, (d) 18 April, (e) 19 April, and (f) 20 April by the ACT experiment and the Ex_AM experiment. Note: Different colors are for different times (blue: 10:00; red: 12:00; yellow: 14:00; green: 16:00). Solid lines are from the ACT experiment and dashed lines are from the Ex_AM experiment. The colored rectangles on the right side demonstrate the PBLH at different times.

has an ~550 m average thickness and could last approximately 5–6 h in the afternoon (Fig. 5b). At a certain supersaturation, the possibility of aerosol being activated as CCN is controlled by the particle diameter, chemical composition and mixing state. The larger the particle size is, the more easily activated the aerosol is (Dusek et al., 2006; Petters and Kreidenweis, 2007). Dusek et al. (2006) proposed that particles smaller than 40 nm typically require extremely high supersaturation for activation. In this study, the averaged critical diameter for activation was 95 nm, 56 nm, 50 nm, and 47 nm when the supersaturation was 0.15%, 0.35%, 0.55% and 0.75%, respectively, based on the method in Furutani et al. (2008). As shown in Fig. S7, when the particle size was greater than ~40 nm (the whisker of the $CCN_{0.35\%}$ boxplot), the particle could be activated with a supersaturation larger than or equal to 0.35%. In addition, it is worth noting that the differences in CCN between the top of the boundary layer and surface, referred to as the $\triangle CCN_{\text{boundary layer top - surface}}$, become more pronounced at higher supersaturations, i.e., the CCN at the top of the boundary layer was on average 28% and 41% higher than that at the surface under the supersaturation of 0.35% and 0.75%, respectively (Fig. S8). Considering the critical diameter at elevated supersaturation (Fig. S7), it is inferred that small particles predominantly contributed to the high CCN layer. As shown in Fig. 5b–c, the $CN_{40–100}$ and $CCN_{0.75\%}$ at the boundary layer top decreased significantly when the nucleation was turned off. Nucleation accounts for 72% of $CN_{40–100}$ and 64% of $CCN_{0.75\%}$ at the top of the boundary layer. Overall, $CCN_{0.55\%}$ and $CCN_{0.75\%}$ were basically consistent with the trend of $CN_{40–100}$ (Figs. 5a–b, S9). Thus, it can be inferred that the high CCN layer at the boundary layer top could be contributed to the increase of $CN_{40–100}$, caused by atmospheric nucleation and the subsequent growth of the newly formed particles.

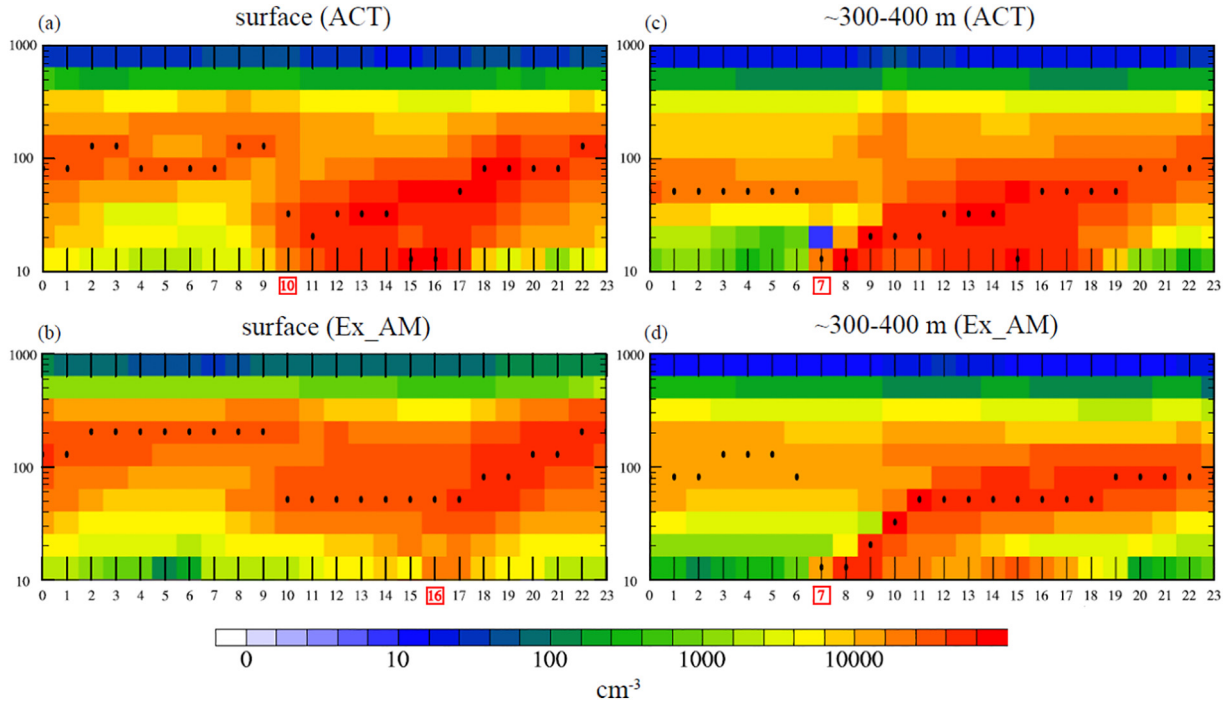

Fig. 4. Modeled particle number size distributions in logarithmic coordinates (a) at the surface for ACT (b) and Ex_AM and (c) ~300–400 m (the PBLH in the morning) for ACT (d) and Ex_AM. Black dots show the representative diameters in the 10–1000 nm diameter range. The red rectangle as well as the inside red number at the abscissa axis denotes the start time of the corresponding NPF event.

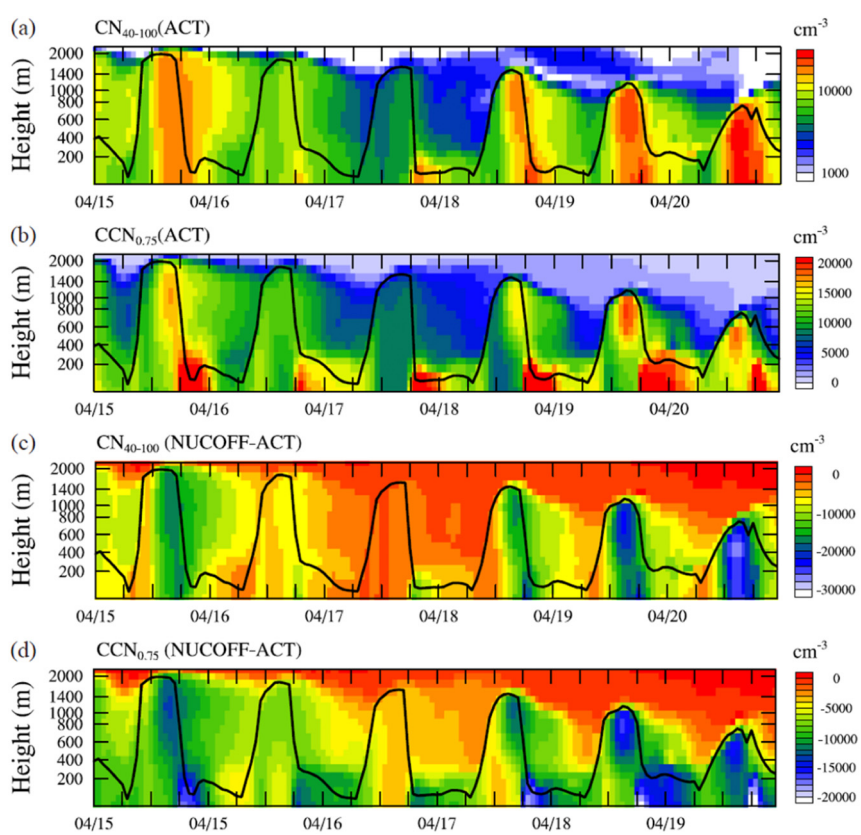

Fig. 5. Times series of (a) $CN_{40–100}$ (b) and $CCN_{0.75}$ in the ACT experiment, differences between NUCOFF and ACT in (c) $CN_{40–100}$ (d) and $CCN_{0.75}$ on 15–20 April. The solid black lines denote the temporal evolution of the PBLH.

3.4.2. Influence of gas mixing on CCN at the top of the PBL

In addition to the test of aerosol vertical mixing, the gas vertical mixing is also discussed in a sensitivity study through switching off (Ex_GM). The high $CN_{40–100}$ layer at the boundary layer top disappeared in the vertical direction in Ex_GM (Fig. 6a). Compared with ACT, $CN_{40–100}$ at ground level in Ex_GM decreased by 5% from 1.4×10^4 cm^{-3} to 1.1×10^4 cm^{-3} while at the boundary layer top, $CN_{40–100}$ decreased more significantly from 1.4×10^4 cm^{-3} to 0.6×10^4 cm^{-3} with a reduction of 47%. Budget diagnostics for condensational growth are utilized to illustrate the effect of gas vertical mixing on particle number concentrations. Fig. 6b–c depicts the condensation (/evaporation) budget term for $CN_{40–100}$. With the aid of budget diagnostics, it was found that $CN_{40–100}$ is mainly contributed by the aerosol chemical module, with a mean contribution of 6.8×10^3 cm^{-3} h^{-1} (Fig. 6b).

In the Ex_GM experiment, due to the lack of gas mixing from the ground, condensable gases at the boundary layer top were significantly reduced. Thus, the contribution of condensational growth to $CN_{40–100}$ decreased, even from a positive contribution to a negative contribution (Fig. 6c). This variation in the contribution of condensation led to the disappearance of the high $CN_{40–100}$. As indicated in Section 3.4.1, $CN_{40–100}$ was closely associated with the high CCN layer at the boundary layer top. As a consequence, the high CCN layer at the boundary layer top where CCN had a significant effect on precipitation also disappeared (Fig. 7). Since the critical activation diameter is larger for $CCN_{0.15\%}$, it is harder for particles to grow up to this size. Thus, $CCN_{0.15\%}$ at the boundary layer top was reduced by 19%, while $CCN_{0.75\%}$ decreased by 43% in Ex_GM (Fig. 7). Overall, it is concluded that the nucleated particles at the boundary layer top grow through the condensation of condensable gases mixing from the ground, and these particles can be potentially activated as CCN as they reach the critical size. The mechanism is schematically illustrated in Fig. 8.

4. Conclusions and uncertainty discussions

This study utilizes WRF-Chem to shed light on NPF processes and vertical mixing at the SORPES in Nanjing on 15–20 April 2018. On 15–20 April, NPF events are captured by DMPS on a daily basis. Through the detailed examination and comparison of the two periods (15–17 April vs. 18–20 April), the latter period exhibits the characteristics of a lower PBLH with weaker PBL mixing, leading to a 30% higher Fuchs surface area at the ground level. Meanwhile, the peak time of nucleation mode particle number concentrations during 18–20 April is delayed by ~1.6 h, implying a postponed start time of NPF.

The results indicate that the fresh particles formed at the top of the boundary layer are transported downward by vertical mixing as the PBL develops. On the days with weaker PBL mixing, the modeled $CN_{10–40}$ at the boundary layer top shows a peak earlier than that at the ground. The elimination of aerosol vertical mixing yields a sharp weakening of NPF strength and delayed the start of NPF at the surface. The phenomenon is primarily attributed to two factors, including the weakened downward transport of particles formed at high altitudes as well as the suppressed upward mixing of particles from the surface, leading to a greater Fuchs surface area and condensational loss of gases and clusters. Newly formed particles can potentially be activated as CCN after hours of growth (Zhu et al., 2019; Gao et al., 2020). On days with weaker PBL mixing, it is difficult for small particles formed at the boundary layer top to transport downward, leading to the appearance of high $CN_{40–100}$ and CCN number concentrations near the boundary layer top. In addition, the condensational growth of particles at the boundary layer top relies on gases from the ground. With the removal of gas vertical mixing, the $CCN_{0.75\%}$ at the boundary layer top decreases by 43%. Through the condensation of condensable gases mixing from the ground, the nucleated particles at the boundary layer top grow up to be potentially activated as CCN and thus exert a profound impact on climate.

This study delineates the linkage between PBL dynamics and NPF, implicating the essential role of aerosol vertical mixing on NPF at the ground. Whereas the existing studies on NPF, particularly from the observational perspective primarily focus on the formation at low altitudes close to the surface, our findings imply an urgent need for a deeper understanding of the transport effect within the PBL, ideally through a full incorporation of observations and simulations.

There are two major uncertainties that need to be addressed in future work. First, in WRF-Chem, H_2SO_4 tends to be overestimated, which also has been reported in other studies as well (Matsui et al., 2011; Cai et al., 2016; Yu et al., 2020). This result indicated that the overestimation of H_2SO_4 (Fig. S4) cannot be fully explained by SO_2, possibly attributed to either measurement bias as pointed out by Neitola et al. (2015) and Yu et al. (2020), or the missing heterogeneous reactions in MOSAIC associated with sulfate (Huang et al., 2014; Xie et al., 2015; Shang et al., 2020). Second, although an ACT mechanism involving H_2SO_4 alone has been applied in this study as well as many previous studies (Matsui et al., 2011; Matsui et al., 2013; Cui et al., 2014; Lupascu et al., 2015; Dong et al., 2019), it is admitted that other precursors have been proposed as being involved in the

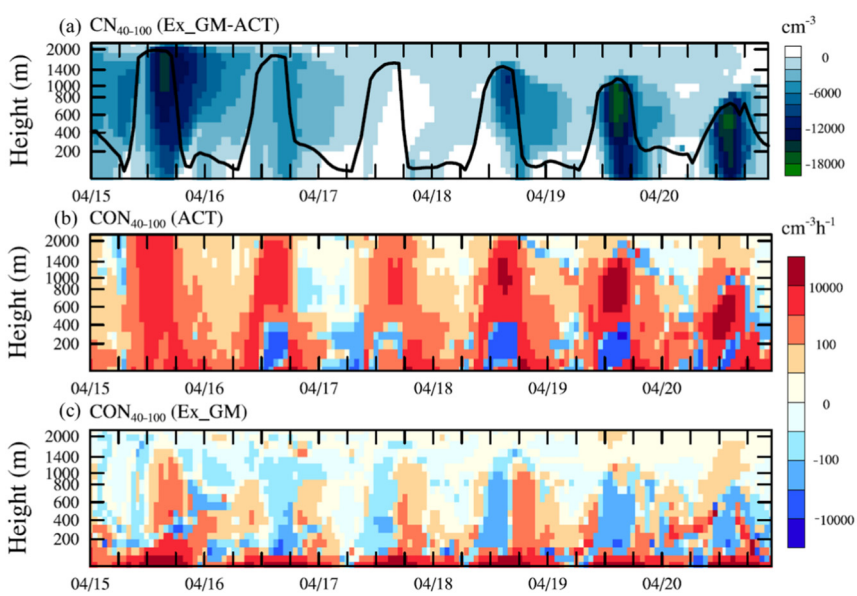

Fig. 6. (a) Time series of the difference in $CN_{40–100}$ between experiments Ex_GM and ACT on 15–20 April; time series of the condensation tendencies for particle number concentrations in the 40–100 nm diameter range by (b) ACT experiment, (c) Ex_GM experiment on 15–20 April.

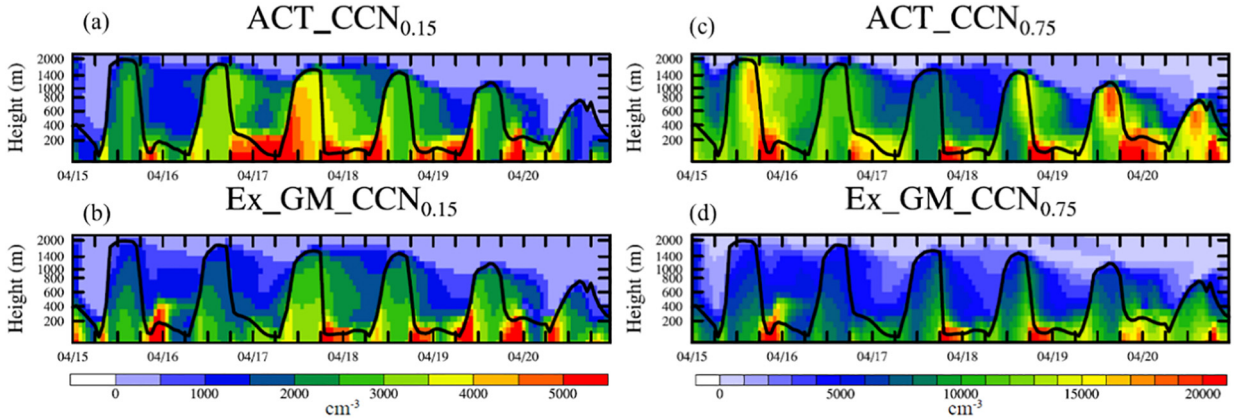

Fig. 7. Time series of (a) $CCN_{0.15}$ by ACT experiment, (b) $CCN_{0.15}$ by Ex_GM, (c) $CCN_{0.75}$ by ACT experiment, (d) $CCN_{0.75}$ by Ex_GM.

formation of the critical nucleus under diverse environments, such as ions (Kirkby et al., 2011; Kirkby et al., 2016), ammonia (Kirkby et al., 2011), amines (Almeida et al., 2013; Bergman et al., 2015; Yao et al., 2018; Cai et al., 2021), and oxidized organic vapors (Schobesberger et al., 2013; Ehn et al., 2014; Riccobono et al., 2014). NPF formation based on other mechanisms deserves more investigation and discussion in future studies.

CRediT authorship contribution statement

Shiyi Lai: Visualization, Formal analysis, Writing - original draft. **Shangfei Hai**: Visualization, Formal analysis, Writing - original draft. **Yang Gao**: Conceptualization, Methodology, Writing - review & editing. **Yuhang Wang**: Methodology, Writing - review & editing. **Lifang Sheng**: Writing - review & editing. **Aura Lupascu**: Formal analysis, Writing - review & editing. **Aijun Ding**: Formal analysis, Writing - review & editing. **Wei Nie**: Writing - review & editing. **Ximeng Qi**: Investigation, Writing - review & editing. **Xin Huang**: Writing - review & editing. **Xuguang Chi**: Investigation. **Chun Zhao**: Formal analysis. **Bin Zhao**: Formal analysis, Writing - review & editing. **Manish Shrivastava**: Formal analysis, Writing - review & editing. **Jerome D. Fast**: Writing - review & editing. **Xiaohong Yao**: Formal analysis, Writing - review & editing. **Huiwang Gao**: Writing - review & editing.

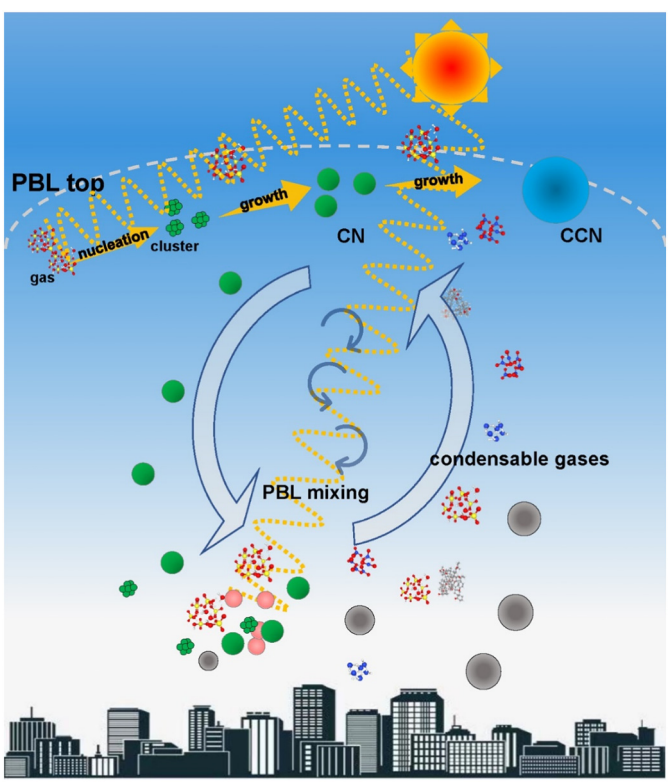

Fig. 8. Schematic illustration of vertical mixing on the new particle formation process. The upper part illustrates the formation and growth of new particles at the boundary layer top. Fresh particles formed at the boundary layer top could be transported downward as the PBL develops. In addition, the Fuchs surface area at the ground is effectively reduced with the evolution of the PBL, which is favorable for the onset of the NPF event at the ground. Sufficient condensable gases at the ground are uplifted by vertical mixing and promote the condensational growth of particles at the boundary layer top.

Declaration of competing interest

The authors declare that they have no known competing financial interests or personal relationships that could have appeared to influence the work reported in this paper.

Acknowledgment

This research was supported by grants from the National Natural Science Foundation of China (91744208, 41805101), and Fundamental Research Funds for the Central Universities (201912012). Chun Zhao was supported by the Fundamental Research Funds for the Central Universities and the Strategic Priority Research Program of Chinese Academy of Sciences (grant XDB41000000). PNNL is operated for DOE by Battelle Memorial Institute under contract DE-AC05-76RL01830. We thank colleagues and students at the School of Atmospheric Sciences at Nanjing University for their contributions to the maintenance of the measurements.

Appendix A. Supplementary data

Supplementary data to this article can be found online at https://doi.org/10.1016/j.scitotenv.2022.154607.

References

Almeida, J., Schobesberger, S., Kurten, A., Ortega, I.K., Kupiainen-Maatta, O., Praplan, A.P., Adamov, A., Amorim, A., Bianchi, F., Breitenlechner, M., et al., 2013. Molecular understanding of sulphuric acid-amine particle nucleation in the atmosphere. Nature 502, 359–363. https://doi.org/10.1038/nature12663.

Bergman, T., Laaksonen, A., Korhonen, H., Malila, J., Dunne, E.M., Mielonen, T., Lehtinen, K.E.J., Kühn, T., Arola, A., Kokkola, H., 2015. Geographical and diurnal features of amine-enhanced boundary layer nucleation. J. Geophys. Res.-Atmos. 120, 9606–9624. https://doi.org/10.1002/2015jd023181.

Bianchi, F., Trostl, J., Junninen, H., Frege, C., Henne, S., Hoyle, C.R., Molteni, U., Herrmann, E., Adamov, A., Bukowiecki, N., et al., 2016. New particle formation in the free troposphere: a question of chemistry and timing. Science 352, 1109–1112. https://doi.org/10.1126/science.aad5456.

Boulon, J., Sellegri, K., Hervo, M., Picard, D., Pichon, J.M., Fréville, P., Laj, P., 2011. Investigation of nucleation events vertical extent: a long term study at two different

altitude sites. Atmos. Chem. Phys. 11, 5625–5639. https://doi.org/10.5194/acp-11-5625-2011.

Brean, J., Harrison, R.M., Shi, Z., Beddows, D.C.S., Acton, W.J.F., Hewitt, C.N., Squires, F.A., Lee, J., 2019. Observations of highly oxidized molecules and particle nucleation in the atmosphere of Beijing. Atmos. Chem. Phys. 19, 14933–14947. https://doi.org/10.5194/acp-19-14933-2019.

Cai, C., Zhang, X., Wang, K., Zhang, Y., Wang, L., Zhang, Q., Duan, F., He, K., Yu, S.-C., 2016. Incorporation of new particle formation and early growth treatments into WRF/Chem: model improvement, evaluation, and impacts of anthropogenic aerosols over East Asia. Atmos. Environ. 124, 262–284. https://doi.org/10.1016/j.atmosenv.2015.05.046.

Cai, R., Yang, D., Fu, Y., Wang, X., Li, X., Ma, Y., Hao, J., Zheng, J., Jiang, J., 2017. Aerosol surface area concentration: a governing factor in new particle formation in Beijing. Atmos. Chem. Phys. 17, 12327–12340. https://doi.org/10.5194/acp-17-12327-2017.

Cai, R., Yan, C., Yang, D., Yin, R., Lu, Y., Deng, C., Fu, Y., Ruan, J., Li, X., Kontkanen, J., et al., 2021. Sulfuric acid–amine nucleation in urban Beijing. Atmos. Chem. Phys. 21, 2457–2468. https://doi.org/10.5194/acp-21-2457-2021.

Carter, W., 2000. Documentation of the SAPRC-99 Chemical Mechanism for VOC Reactivity Assessment. pp. 95–308.

Chen, F., Dudhia, J., 2001. Coupling an advanced land surface-hydrology model with the Penn State-NCAR MM5 modeling system. Part I: model implementation and sensitivity. Mon. Weather Rev. 129, 569–585. https://doi.org/10.1175/1520-0493(2001)129<0569:Caalsh>2.0.Co;2.

Chen, H., Hodshire, A.L., Ortega, J., Greenberg, J., McMurry, P.H., Carlton, A.G., Pierce, J.R., Hanson, D.R., Smith, J.N., 2018. Vertically resolved concentration and liquid water content of atmospheric nanoparticles at the US DOE Southern Great Plains site. Atmos. Chem. Phys. 18, 311–326. https://doi.org/10.5194/acp-18-311-2018.

Chen, X., Yang, W., Wang, Z., Li, J., Hu, M., An, J., Wu, Q., Wang, Z., Chen, H., Wei, Y., et al., 2019. Improving new particle formation simulation by coupling a volatility-basis set (VBS) organic aerosol module in NAQPMS + APM. Atmos. Environ. 204, 1–11. https://doi.org/10.1016/j.atmosenv.2019.01.053.

Chu, B., Kerminen, V.-M., Bianchi, F., Yan, C., Petäjä, T., Kulmala, M., 2019. Atmospheric new particle formation in China. Atmos. Chem. Phys. 19, 115–138. https://doi.org/10.5194/acp-19-115-2019.

Crumeyrolle, S., Manninen, H.E., Sellegri, K., Roberts, G., Gomes, L., Kulmala, M., Weigel, R., Laj, P., Schwarzenboeck, A., 2010. New particle formation events measured on board the ATR-42 aircraft during the EUCAARI campaign. Atmos. Chem. Phys. 10, 6721–6735. https://doi.org/10.5194/acp-10-6721-2010.

Cui, Y.Y., Hodzic, A., Smith, J.N., Ortega, J., Brioude, J., Matsui, H., Levin, E.J.T., Turnipseed, A., Winkler, P., de Foy, B., 2014. Modeling ultrafine particle growth at a pine forest site influenced by anthropogenic pollution during BEACHON-RoMBAS 2011. Atmos. Chem. Phys. 14, 11011–11029. https://doi.org/10.5194/acp-14-11011-2014.

Deng, C., Cai, R., Yan, C., Zheng, J., Jiang, J., 2020. Formation and growth of sub-3 nm particles in megacities: impact of background aerosols. Faraday Discuss. https://doi.org/10.1039/d0fd00083c.

Ding, A.J., Fu, C.B., Yang, X.Q., Sun, J.N., Zheng, L.F., Xie, Y.N., Herrmann, E., Nie, W., Petäjä, T., Kerminen, V.M., et al., 2013. Ozone and fine particle in the western Yangtze River Delta: an overview of 1 yr data at the SORPES station. Atmos. Chem. Phys. 13, 5813–5830. https://doi.org/10.5194/acp-13-5813-2013.

Dong, C., Matsui, H., Spak, S., Kalafut-Pettibone, A., Stanier, C., 2019. Impacts of new particle formation on short-term meteorology and air quality as determined by the NPF-explicit WRF-Chem in the midwestern United States. Aerosol Air Qual. Res. 19, 204–220. https://doi.org/10.4209/aaqr.2018.05.0163.

Du, Q., Zhao, C., Zhang, M., Dong, X., Chen, Y., Liu, Z., Hu, Z., Zhang, Q., Li, Y., Yuan, R., et al., 2020. Modeling diurnal variation of surface PM_{2.5} concentrations over East China with WRF-Chem: impacts from boundary-layer mixing and anthropogenic emission. Atmos. Chem. Phys. 20, 2839–2863. https://doi.org/10.5194/acp-20-2839-2020.

Dunne, E.M., Gordon, H., Kurten, A., Almeida, J., Duplissy, J., Williamson, C., Ortega, I.K., Pringle, K.J., Adamov, A., Baltensperger, U., et al., 2016. Global atmospheric particle formation from CERN CLOUD measurements. Science 354, 1119–1124. https://doi.org/10.1126/science.aaf2649.

Dusek, U., Frank, G.P., Hildebrandt, L., Curtius, J., Schneider, J., Walter, S., Chand, D., Drewnick, F., Hings, S., Jung, D., Borrmann, S., Andreae, M.O., 2006. Size matters more than chemistry for cloud nucleating ability of aerosol particles. Science 312, 1375–1378.

Ehn, M., Thornton, J.A., Kleist, E., Sipila, M., Junninen, H., Pullinen, I., Springer, M., Rubach, F., Tillmann, R., Lee, B., et al., 2014. A large source of low-volatility secondary organic aerosol. Nature 506, 476–479. https://doi.org/10.1038/nature13032.

Emery, C., Tai, E., 2001. Enhanced Meteorological Modeling and Performance Evaluation for Two Texas Ozone Episodes. Prepared for the Texas natural resource conservation commissionENVIRON International Corporation.

Fanourgakis, G.S., Kanakidou, M., Nenes, A., Bauer, S.E., Bergman, T., Carslaw, K.S., Grini, A., Hamilton, D.S., Johnson, J.S., Karydis, V.A., et al., 2019. Evaluation of global simulations of aerosol particle and cloud condensation nuclei number, with implications for cloud droplet formation. Atmos. Chem. Phys. 19, 8591–8617. https://doi.org/10.5194/acp-19-8591-2019.

Fast, J.D., Gustafson, W.I., Easter, R.C., Zaveri, R.A., Barnard, J.C., Chapman, E.G., Grell, G.A., Peckham, S.E., 2006. Evolution of ozone, particulates, and aerosol direct radiative forcing in the vicinity of Houston using a fully coupled meteorology-chemistry-aerosol model. J. Geophys. Res.-Atmos. 111, 29. https://doi.org/10.1029/2005jd006721.

Furutani, H., Dall'osto, M., Roberts, G.C., Prather, K.A., 2008. Assessment of the relative importance of atmospheric aging on CCN activity derived from field observations. Atmos. Environ. 42, 3130–3142. https://doi.org/10.1016/j.atmosenv.2007.09.024.

Gao, Y., Zhang, D., Wang, J., Gao, H., Yao, X., 2020. Variations in N-cn and N-ccn over marginal seas in China related to marine traffic emissions, new particle formation and aerosol aging. Atmos. Chem. Phys. 20, 9665–9677. https://doi.org/10.5194/acp-20-9665-2020.

Gao, Y., Yan, F., Ma, M., Ding, A., Liao, H., Wang, S., Wang, X., Zhao, B., Cai, W., Su, H., et al., 2021. Unveiling the dipole synergic effect of biogenic and anthropogenic emissions on ozone concentrations. Sci. Total Environ. 151722. https://doi.org/10.1016/j.scitotenv.2021.151722.

Grell, G.A., 1993. Prognostic evaluation of assumptions used by cumulus parameterazations. Mon. Weather Rev. 121, 764–787. https://doi.org/10.1175/1520-0493(1993)121<0764:Peoaub>2.0.Co;2.

Grell, G.A., Peckham, S.E., Schmitz, R., McKeen, S.A., Frost, G., Skamarock, W.C., Eder, B., 2005. Fully coupled "online" chemistry within the WRF model. Atmos. Environ. 39, 6957–6975. https://doi.org/10.1016/j.atmosenv.2005.04.027.

Guenther, A., Karl, T., Harley, P., Wiedinmyer, C., Palmer, P.I., Geron, C., 2006. Estimates of global terrestrial isoprene emissions using MEGAN (Model of Emissions of Gases and Aerosols from Nature). Atmos. Chem. Phys. 6, 3181–3210. https://doi.org/10.5194/acp-6-3181-2006.

Herrmann, E., Ding, A., Kerminen, V.M., Petäjä, T., Yang, X., Sun, J., Qi, X., Manninen, H., Hakala, J., Nieminen, T., et al., 2014. Aerosols and nucleation in eastern China: first insights from the new SORPES-NJU station. Atmos. Chem. Phys. 14, 2169–2183. https://doi.org/10.5194/acp-14-2169-2014.

Hong, S.Y., Noh, Y., Dudhia, J., 2006. A new vertical diffusion package with an explicit treatment of entrainment processes. Mon. Weather Rev. 134, 2318–2341. https://doi.org/10.1175/mwr3199.1.

Huang, X., Song, Y., Zhao, C., Li, M.M., Zhu, T., Zhang, Q., Zhang, X.Y., 2014. Pathways of sulfate enhancement by natural and anthropogenic mineral aerosols in China. J. Geophys. Res.-Atmos. 119, 14165–14179. https://doi.org/10.1002/2014jd022301.

Huang, X., Zhou, L., Ding, A., Qi, X., Nie, W., Wang, M., Chi, X., Petäjä, T., Kerminen, V.-M., Roldin, P., et al., 2016. Comprehensive modelling study on observed new particle formation at the SORPES station in Nanjing, China. Atmos. Chem. Phys. 16, 2477–2492. https://doi.org/10.5194/acp-16-2477-2016.

Iacono, M.J., Delamere, J.S., Mlawer, E.J., Shephard, M.W., Clough, S.A., Collins, W.D., 2008. Radiative forcing by long-lived greenhouse gases: calculations with the AER radiative transfer models. J. Geophys. Res.-Atmos. 113, 8. https://doi.org/10.1029/2008jd009944.

Jimenez, P.A., Dudhia, J., Gonzalez-Rouco, J.F., Navarro, J., Montavez, J.P., Garcia-Bustamante, E., 2012. A revised scheme for the WRF surface layer formulation. Mon. Weather Rev. 140, 898–918. https://doi.org/10.1175/mwr-d-11-00056.1.

Kazil, J., Stier, P., Zhang, K., Quaas, J., Kinne, S., O'Donnell, D., Rast, S., Esch, M., Ferrachat, S., Lohmann, U., et al., 2010. Aerosol nucleation and its role for clouds and Earth's radiative forcing in the aerosol-climate model ECHAM5-HAM. Atmos. Chem. Phys. 10, 10733–10752. https://doi.org/10.5194/acp-10-10733-2010.

Kerminen, V.-M., Pirjola, L., Kulmala, M., 2001. How significantly does coagulational scavenging limit atmospheric particle production? J. Geophys. Res.-Atmos. 106, 24119–24125. https://doi.org/10.1029/2001jd000322.

Kirkby, J., Curtius, J., Almeida, J., Dunne, E., Duplissy, J., Ehrhart, S., Franchin, A., Gagne, S., Ickes, L., Kurten, A., et al., 2011. Role of sulphuric acid, ammonia and galactic cosmic rays in atmospheric aerosol nucleation. Nature 476, 429–U477. https://doi.org/10.1038/nature10343.

Kirkby, J., Duplissy, J., Sengupta, K., Frege, C., Gordon, H., Williamson, C., Heinritzi, M., Simon, M., Yan, C., Almeida, J., et al., 2016. Ion-induced nucleation of pure biogenic particles. Nature 533, 521–526. https://doi.org/10.1038/nature17953.

Kulmala, M., 2003. How particles nucleate and grow. Science 302, 1000–1001. https://doi.org/10.1126/science.1090848.

Kulmala, M., Riipinen, I., Sipilä, M., Manninen, H.E., Petäjä, T., Junninen, H., Maso, M.D., Mordas, G., Mirme, A., Vana, M., et al., 2007. Toward direct measurement of atmospheric nucleation. Science 318, 89–92. https://doi.org/10.1126/science.1144124.

Kulmala, M., Petaja, T., Nieminen, T., Sipila, M., Manninen, H.E., Lehtipalo, K., Dal Maso, M., Aalto, P.P., Junninen, H., Paasonen, P., et al., 2012. Measurement of the nucleation of atmospheric aerosol particles. Nat. Protoc. 7, 1651–1667. https://doi.org/10.1038/nprot.2012.091.

Kulmala, M., Maso, M.D., Mäkelä, J.M., Pirjola, L., Väkevä, M., Aalto, P., Miikkulainen, P., Hämeri, K., O'dowd, C.D., 2016. On the formation, growth and composition of nucleation mode particles. Tellus Ser. B-Chem. Phys. Meteorol. 53, 479–490. https://doi.org/10.3402/tellusb.v53i4.16622.

Lampilahti, J., Manninen, H.E., Leino, K., Väänänen, R., Manninen, A., Buenrostro Mazon, S., Nieminen, T., Leskinen, M., Enroth, J., Bister, M., et al., 2020. Roll vortices induce new particle formation bursts in the planetary boundary layer. Atmos. Chem. Phys. 20, 11841–11854. https://doi.org/10.5194/acp-20-11841-2020.

Lee, S.H., Reeves, J.M., Wilson, J.C., Hunton, D.E., Viggiano, A.A., Miller, T.M., Ballenthin, J.O., Lait, L.R., 2003. Particle formation by ion nucleation in the upper troposphere and lower stratosphere. Science 301, 1886–1889. https://doi.org/10.1126/science.1087236.

Leng, C., Zhang, Q., Tao, J., Zhang, H., Zhang, D., Xu, C., Li, X., Kong, L., Cheng, T., Zhang, R., et al., 2014. Impacts of new particle formation on aerosol cloud condensation nuclei (CCN) activity in Shanghai: case study. Atmos. Chem. Phys. 14, 11353–11365. https://doi.org/10.5194/acp-14-11353-2014.

Lin, Y.H., Zhang, H.F., Pye, H.O.T., Zhang, Z.F., Marth, W.J., Park, S., Arashiro, M., Cui, T.Q., Budisulistiorini, H., Sexton, K.G., et al., 2013. Epoxide as a precursor to secondary organic aerosol formation from isoprene photooxidation in the presence of nitrogen oxides. Proc. Natl. Acad. Sci. U. S. A. 110, 6718–6723. https://doi.org/10.1073/pnas.1221150110.

Lupascu, A., Easter, R., Zaveri, R., Shrivastava, M., Pekour, M., Tomlinson, J., Yang, Q., Matsui, H., Hodzic, A., Zhang, Q., et al., 2015. Modeling particle nucleation and growth over northern California during the 2010 CARES campaign. Atmos. Chem. Phys. 15, 12283–12313. https://doi.org/10.5194/acp-15-12283-2015.

Ma, M., Gao, Y., Wang, Y., Zhang, S., Leung, L.R., Liu, C., Wang, S., Zhao, B., Chang, X., Su, H., et al., 2019. Substantial ozone enhancement over the North China Plain from increased biogenic emissions due to heat waves and land cover in summer 2017. Atmos. Chem. Phys. 19, 12195–12207. https://doi.org/10.5194/acp-19-12195-2019.

Ma, M., Gao, Y., Ding, A., Su, H., Liao, H., Wang, S., Wang, X., Zhao, B., Zhang, S., Fu, P., et al., 2022. Development and assessment of a high-resolution biogenic emission inventory from urban green spaces in China. Environ. Sci. Technol. 56, 175–184. https://doi.org/10.1021/acs.est.1c06170.

Manninen, H.E., Petaja, T., Asmi, E., Riipinen, I., Nieminen, T., Mikkila, J., Horrak, U., Mirme, A., Mirme, S., Laakso, L., et al., 2009. Long-term field measurements of charged and neutral clusters using Neutral cluster and Air Ion Spectrometer (NAIS). Boreal Environ. Res. 14, 591–605.

Matsui, H., Koike, M., Kondo, Y., Takegawa, N., Wiedensohler, A., Fast, J.D., Zaveri, R.A., 2011. Impact of new particle formation on the concentrations of aerosols and cloud condensation nuclei around Beijing. J. Geophys. Res.-Atmos. 116, 19. https://doi.org/10.1029/2011jd016025.

Matsui, H., Koike, M., Takegawa, N., Kondo, Y., Takami, A., Takamura, T., Yoon, S., Kim, S.W., Lim, H.C., Fast, J.D., 2013. Spatial and temporal variations of new particle formation in East Asia using an NPF-explicit WRF-chem model: north-south contrast in new particle formation frequency. J. Geophys. Res.-Atmos. 118, 11647–11663. https://doi.org/10.1002/jgrd.50821.

Morrison, H., Thompson, G., Tatarskii, V., 2009. Impact of cloud microphysics on the development of trailing stratiform precipitation in a simulated squall line: comparison of one- and two-moment schemes. Mon. Weather Rev. 137, 991–1007. https://doi.org/10.1175/2008mwr2556.1.

Neitola, K., Brus, D., Makkonen, U., Sipilä, M., Mauldin Iii, R.L., Sarnela, N., Jokinen, T., Lihavainen, H., Kulmala, M., 2015. Total sulfate vs. sulfuric acid monomer concenterations in nucleation studies. Atmos. Chem. Phys. 15, 3429–3443. https://doi.org/10.5194/acp-15-3429-2015.

O'Dowd, C.D., Jimenez, J.L., Bahreini, R., Flagan, R.C., Seinfeld, J.H., Hämeri, K., Pirjola, L., Kulmala, M., Jennings, S.G., Hoffmann, T., 2002. Marine aerosol formation from biogenic iodine emissions. Nature 417, 632–636.

Petters, M.D., Kreidenweis, S.M., 2007. A single parameter representation of hygroscopic growth and cloud condensation nucleus activity. Atmos. Chem. Phys. 7, 1961–1971. https://doi.org/10.5194/acp-7-1961-2007.

Platis, A., Altstadter, B., Wehner, B., Wildmann, N., Lampert, A., Hermann, M., Birmili, W., Bange, J., 2016. An observational case study on the influence of atmospheric boundary-layer dynamics on new particle formation. Bound.-Layer Meteor. 158, 67–92. https://doi.org/10.1007/s10546-015-0084-y.

Qi, X., Ding, A., Nie, W., Petäjä, T., Kerminen, V.M., Herrmann, E., Xie, Y., Zheng, L., Manninen, H., Aalto, P., et al., 2015. Aerosol size distribution and new particle formation in the western Yangtze River Delta of China: 2 years of measurements at the SORPES station. Atmos. Chem. Phys. 15, 12445–12464. https://doi.org/10.5194/acp-15-12445-2015.

Qi, X., Ding, A., Roldin, P., Xu, Z., Zhou, P., Sarnela, N., Nie, W., Huang, X., Rusanen, A., Ehn, M., et al., 2018. Modelling studies of HOMs and their contributions to new particle formation and growth: comparison of boreal forest in Finland and a polluted environment in China. Atmos. Chem. Phys. 18, 11779–11791. https://doi.org/10.5194/acp-18-11779-2018.

Qi, X., Ding, A., Nie, W., Chi, X., Huang, X., Xu, Z., Wang, T., Wang, Z., Wang, J., Sun, P., et al., 2019. Direct measurement of new particle formation based on tethered airship around the top of the planetary boundary layer in eastern China. Atmos. Environ. 209, 92–101. https://doi.org/10.1016/j.atmosenv.2019.04.024.

Riccobono, F., Schobesberger, S., Scott, C.E., Dommen, J., Ortega, I.K., Rondo, L., Almeida, J., Amorim, A., Bianchi, F., Breitenlechner, M., et al., 2014. Oxidation products of biogenic emissions contribute to nucleation of atmospheric particles. Science 344, 717–721. https://doi.org/10.1126/science.1243527.

Rose, C., Sellegri, K., Freney, E., Dupuy, R., Colomb, A., Pichon, J.M., Ribeiro, M., Bourianne, T., Burnet, F., Schwarzenboeck, A., 2015. Airborne measurements of new particle formation in the free troposphere above the Mediterranean Sea during the HYMEX campaign. Atmos. Chem. Phys. 15, 10203–10218. https://doi.org/10.5194/acp-15-10203-2015.

Saha, S., Moorthi, S., Wu, X., Wang, J., Nadiga, S., Tripp, P., Behringer, D., Hou, Y.-T., Chuang, H.-y., Iredell, M., et al., 2014. The NCEP climate forecast system version 2. J. Clim. 27, 2185–2208. https://doi.org/10.1175/JCLI-D-12-00823.1.

Salma, I., Németh, Z., Kerminen, V.-M., Aalto, P., Nieminen, T., Weidinger, T., Molnár, Á., Imre, K., Kulmala, M., 2016. Regional effect on urban atmospheric nucleation. Atmos. Chem. Phys. 16, 8715–8728. https://doi.org/10.5194/acp-16-8715-2016.

Schobesberger, S., Junninen, H., Bianchi, F., Lonn, G., Ehn, M., Lehtipalo, K., Dommen, J., Ehrhart, S., Ortega, I.K., Franchin, A., et al., 2013. Molecular understanding of atmospheric particle formation from sulfuric acid and large oxidized organic molecules. Proc. Natl. Acad. Sci. U. S. A. 110, 17223–17228. https://doi.org/10.1073/pnas.1306973110.

Shang, D., Peng, J., Guo, S., Wu, Z., Hu, M., 2020. Secondary aerosol formation in winter haze over the Beijing-Tianjin-Hebei Region, China. Front. Env. Sci. Eng. 15. https://doi.org/10.1007/s11783-020-1326-x.

Shen, X., Sun, J., Zhang, X., Zhang, Y., Zhang, L., Fan, R., 2016. Key features of new particle formation events at background sites in China and their influence on cloud condensation nuclei. Front. Env. Sci. Eng. 10. https://doi.org/10.1007/s11783-016-0833-2.

Shrivastava, M., Fast, J., Easter, R., Gustafson, W.I., Zaveri, R.A., Jimenez, J.L., Saide, P., Hodzic, A., 2011. Modeling organic aerosols in a megacity: comparison of simple and complex representations of the volatility basis set approach. Atmos. Chem. Phys. 11, 6639–6662. https://doi.org/10.5194/acp-11-6639-2011.

Sipila, M., Berndt, T., Petaja, T., Brus, D., Vanhanen, J., Stratmann, F., Patokoski, J., Mauldin, R.L., Hyvarinen, A.P., Lihavainen, H., et al., 2010. The role of sulfuric acid in atmospheric nucleation. Science 327, 1243–1246. https://doi.org/10.1126/science.1180315.

Solomon, S., Manning, M., Marquis, M., Qin, D., 2007. Climate Change 2007-The Physical Science Basis: Working Group I Contribution to the Fourth Assessment Report of the IPCC. Cambridge university press.

Stratmann, F., Siebert, H., Spindler, G., Wehner, B., Althausen, D., Heintzenberg, J., Hellmuth, O., Rinke, R., Schmieder, U., Seidel, C., et al., 2003. New-particle formation events in a continental boundary layer: first results from the SATURN experiment. Atmos. Chem. Phys. 3, 1445–1459. https://doi.org/10.5194/acp-3-1445-2003.

Surratt, J.D., Chan, A.W.H., Eddingsaas, N.C., Chan, M.N., Loza, C.L., Kwan, A.J., Hersey, S.P., Flagan, R.C., Wennberg, P.O., Seinfeld, J.H., 2010. Reactive intermediates revealed in secondary organic aerosol formation from isoprene. Proc. Natl. Acad. Sci. U. S. A. 107, 6640–6645. https://doi.org/10.1073/pnas.0911114107.

Tesche, T.W., McNally, D.E., Tremback, C., 2002. Operational Evaluation of the MM5 Meteorological Model Over the Continental United States: Protocol for Annual and Episodic Evaluation.

Tewari, M., Chen, F., Wang, W., Dudhia, J., LeMone, M.A., Mitchell, K., Ek, M., Gayno, G., Wegiel, J., C., a.R.H., 2004. Implementation and Verification of the Unified NOAH land Surface Model in the WRF Model.

Turco, R.P., Zhao, J.-X., Yu, F., 1998. A new source of tropospheric aerosols: ion-ion recombination. Geophys. Res. Lett. 25, 635–638. https://doi.org/10.1029/98gl00253.

US EPA, 2007. Guidance on the Use of Models and Other Analyses for Demonstrating Attainment of Air Quality Goals for Ozone, PM2.5. and Regional Haze. EPA-454/B-07e002.

Wang, M., Penner, J.E., 2009. Aerosol indirect forcing in a global model with particle nucleation. Atmos. Chem. Phys. 9, 239–260. https://doi.org/10.5194/acp-9-239-2009.

Wehner, B., Siebert, H., Ansmann, A., Ditas, F., Seifert, P., Stratmann, F., Wiedensohler, A., Apituley, A., Shaw, R.A., Manninen, H.E., et al., 2010. Observations of turbulence-induced new particle formation in the residual layer. Atmos. Chem. Phys. 10, 4319–4330. https://doi.org/10.5194/acp-10-4319-2010.

Westervelt, D.M., Pierce, J.R., Adams, P.J., 2014. Analysis of feedbacks between nucleation rate, survival probability and cloud condensation nuclei formation. Atmos. Chem. Phys. 14, 5577–5597. https://doi.org/10.5194/acp-14-5577-2014.

Williamson, C.J., Kupc, A., Axisa, D., Bilsback, K.R., Bui, T., Campuzano-Jost, P., Dollner, M., Froyd, K.D., Hodshire, A.L., Jimenez, J.L., et al., 2019. A large source of cloud condensation nuclei from new particle formation in the tropics. Nature 574, 399–403. https://doi.org/10.1038/s41586-019-1638-9.

Wu, H., Li, Z., Li, H., Luo, K., Yuying, W., Yan, P., Hu, F., Zhang, F., Sun, Y., Shang, D., et al., 2020. The impact of the atmospheric turbulence-development tendency on new particle formation: a common finding on three continents. Natl. Sci. Rev. 1-11. https://doi.org/10.1093/nsr/nwaa157.

Xie, Y., Ding, A., Nie, W., Mao, H., Qi, X., Huang, X., Xu, Z., Kerminen, V.-M., Petäjä, T., Chi, X., et al., 2015. Enhanced sulfate formation by nitrogen dioxide: implications from in situ observations at the SORPES station. J. Geophys. Res.-Atmos. 120, 12679–12694. https://doi.org/10.1002/2015jd023607.

Xu, Z., Hang, X., Nie, W., Shen, Y., Zheng, L., Xie, Y., Wang, T., Ding, K., Liu, L., Zhou, D., Qi, X., Ding, A., 2018. Impact of Biomass Burning and Vertical Mixing of Residual-Layer Aged Plumes on Ozone in the Yangtze River Delta, China: A Tethered-Balloon Measurement and Modeling Study of a Multiday Ozone Episode. Journal of Geophysical Research: Atmospheres https://doi.org/10.1029/2018jd028994.

Yao, L., Garmash, O., Bianchi, F., Zheng, J., Yan, C., Kontkanen, J., Junninen, H., Mazon, S.B., Ehn, M., Paasonen, P., et al., 2018. Atmospheric new particle formation from sulfuric acid and amines in a Chinese megacity. Science 361, 278+. https://doi.org/10.1126/science.aao4839.

Yu, F., Luo, G., 2009. Simulation of particle size distribution with a global aerosol model: contribution of nucleation to aerosol and CCN number concentrations. Atmos. Chem. Phys. 9, 7691–7710. https://doi.org/10.5194/acp-9-7691-2009.

Yu, F., Luo, G., Nair, A.A., Schwab, J.J., Sherman, J.P., Zhang, Y., 2020. Wintertime new particle formation and its contribution to cloud condensation nuclei in the Northeastern United States. Atmos. Chem. Phys. 20, 2591–2601. https://doi.org/10.5194/acp-20-2591-2020.

Zaveri, R.A., Easter, R.C., Fast, J.D., Peters, L.K., 2008. Model for Simulating Aerosol Interactions and Chemistry (MOSAIC). J. Geophys. Res. 113. https://doi.org/10.1029/2007jd008782.

Zhang, R.Y., Khalizov, A., Wang, L., Hu, M., Xu, W., 2012. Nucleation and growth of nanoparticles in the atmosphere. Chem. Rev. 112, 1957–2011. https://doi.org/10.1021/cr2001756.

Zhao, B., Shrivastava, M., Donahue, N.M., Gordon, H., Schervish, M., Shilling, J.E., Zaveri, R.A., Wang, J., Andreae, M.O., Zhao, C., et al., 2020. High concentration of ultrafine particles in the Amazon free troposphere produced by organic new particle formation. Proc. Natl. Acad. Sci. U. S. A. 117, 25344–25351. https://doi.org/10.1073/pnas.2006716117.

Zhu, B., Wang, H., Shen, L., Kang, H., Yu, X., 2013. Aerosol spectra and new particle formation observed in various seasons in Nanjing. Adv. Atmos. Sci. 30, 1632–1644. https://doi.org/10.1007/s00376-013-2202-4.

Zhu, Y., Li, K., Shen, Y., Gao, Y., Liu, X., Yu, Y., Gao, H., Yao, X., 2019. New particle formation in the marine atmosphere during seven cruise campaigns. Atmospheric Chemistry and Physics https://doi.org/10.5194/acp-19-89-2019.

Zhu, Y., Sabaliauskas, K., Liu, X., Meng, H., Gao, H., Jeong, C.-H., Evans, G.J., Yao, X., 2014. Comparative analysis of new particle formation events in less and severely polluted urban atmosphere. Atmos. Environ. 98, 655–664. https://doi.org/10.1016/j.atmosenv.2014.09.043.